Journal of Hydrology 523 (2015) 475–488

Contents lists available at ScienceDirect

Journal of Hydrology

journal homepage: www.elsevier.com/locate/jhydrol

Quantifying spatiotemporal dynamics of root-zone soil water in a mixed forest on subtropical coastal sand dune using surface ERT and spatial TDR

Junliang Fan [a,b,*], Alexander Scheuermann [a], Adrien Guyot [a,b], Thomas Baumgartl [c], David A. Lockington [a,b]

[a] School of Civil Engineering, The University of Queensland, Brisbane 4072, Australia
[b] National Center for Groundwater Research and Training, Adelaide 5001, Australia
[c] Center for Mined Land Rehabilitation, The University of Queensland, Brisbane 4072, Australia

ARTICLE INFO

Article history:
Received 8 July 2014
Received in revised form 26 January 2015
Accepted 28 January 2015
Available online 10 February 2015
This manuscript was handled by Peter K. Kitanidis, Editor-in-Chief, with the assistance of J.A. Huisman, Associate Editor

Keywords:
Surface electrical resistivity tomography (surface ERT)
Spatial time domain reflectometry (spatial TDR)
Rainfall redistribution
Root water uptake
Coastal sand dune forest

SUMMARY

We jointly used surface electrical resistivity tomography (surface ERT) and spatial time domain reflectometry (spatial TDR) to quantify spatial patterns and seasonal dynamics of root-zone soil water under three contrasting vegetation covers in a sand dune forest of subtropical coastal Australia. We wanted to obtain a better understanding of the applicability of both techniques in these environments as well as investigate vegetation–soil water interactions. Soil temperature and topographic changes were taken into account in soil resistivity interpretation. The results demonstrated the capability of both surface ERT and spatial TDR to spatially monitor root-zone soil water dynamics, with root mean square error (RMSE) <0.018 $cm^3\ cm^{-3}$ and absolute deviation <0.034 $cm^3\ cm^{-3}$ between gravimetrically derived water content and those derived by the two geophysical techniques. Soil water was depleted to low levels during the dry season but quickly replenished with onset of the wet season. Soil water content profiles revealed obvious differences in water dynamics of the dune sands under different vegetation covers, with highest infiltration and deep drainage under the grassland compared with tree cover. The spatial variation in soil water content due to rainfall interception by trees, root water uptake and preferential infiltration associated with stemflow could be detected by the joint use of surface ERT and spatial TDR. We conclude that surface ERT can be an effective method for quantifying two-dimensional root-zone soil water dynamics and understanding the hydrological processes in these sand dune environments, if complemented by the one-dimensional high-resolution soil water measurements from spatial TDR.

1. Introduction

Significant resources of generally high quality groundwater are located in sandy coastal environments around the world. In these aquifer systems, forest type and distribution strongly affect the local groundwater balance, i.e. recharge and discharge (Bosch and Hewlett, 1982; Zhang et al., 2001; Ford et al., 2011). Their effect on recharge distribution is mainly due to rainfall interception by the canopy and soil water extraction by roots. Recharge patterns will also reflect the presence of preferential flow paths and variations in topography which can be influenced by vegetation. Characterizing the spatiotemporal dynamics of root-zone soil water is useful for understanding these vegetation-associated hydrological processes (Vereecken et al., 2008, 2013). A detailed study of spatiotemporal heterogeneity and drivers of root-zone soil water dynamics is also necessary for appropriate design and calibration of groundwater management models and more specifically soil-vegetation-atmosphere models (Western et al., 2003). Nevertheless, quantitatively evaluating spatial and temporal evolutions of subsurface water content with high spatial and temporal resolution remains challenging in practice (Jayawickreme et al., 2008).

Time domain reflectometry (TDR) and capacitance probes are commonly used to measure soil water at shallow depths (Schwartz et al., 2008; Calamita et al., 2012; Beff et al., 2013). However, these methods only provide information about a relatively small volume of soil, often limited to a few centimeters around the sensors (Ferré et al., 1998). Monitoring spatial patterns of soil water at a larger scale using a network of such point-scale sensors can be expensive and impractical. Satellite and airborne remote sensing methods are useful to detect soil water distribution at regional scale, but its investigation depth is restricted to a few

* Corresponding author at: School of Civil Engineering, The University of Queensland, Brisbane 4072, Australia.
E-mail address: nwwfjl@gmail.com (J. Fan).

http://dx.doi.org/10.1016/j.jhydrol.2015.01.064
0022-1694/

centimeters and the spatial resolution is too coarse (Robinson et al., 2012). At intermediate scales (decameter to hectometer), geophysical techniques, such as electromagnetic induction (EMI), ground penetrating radar (GPR) and electrical resistivity tomography (ERT), have proven to be promising alternatives to infer soil water down to several meters (e.g., Huisman et al., 2003; Brunet et al., 2010; Robinson et al., 2012; Steelman et al., 2012; Brillante et al., 2014). EMI is useful for mapping the horizontal distribution of subsurface electrical resistivity, but it gives little information on its vertical distributions (Robinson et al., 2008). Surface-based GPR is difficult to apply in forests due to the presence of vegetation cover on the soil surface and a more sophisticated calculation is required when interpreting the data. Instead, surface ERT is a non-invasive tool to produce two- or three-dimensional (2D or 3D) variations of the subsurface electrical resistivity, which can be closely related to changes in soil water content (Zhou et al., 2001).

Surface ERT has been widely used for hydrological investigations, *e.g.* water infiltration (Michot et al., 2003; French and Binley, 2004; Lehmann et al., 2013), potential recharge (Schwartz and Schreiber, 2009) and groundwater fluctuation (Yamakawa et al., 2012). Recently, it has also been deployed to explore vegetation and soil water interactions. For example, Jayawickreme et al. (2008, 2010) identified large difference in soil water distributions beneath adjacent forest and grassland biomes. Surface ERT has also been used to monitor soil water dynamics influenced by root water uptake by agricultural crops, *i.e.* corn and sorghum (Srayeddin and Doussan, 2009). Beff et al. (2013) monitored 3D soil water distributions in a corn field using surface ERT combined with cross-borehole ERT. However, no studies have used time-lapse surface ERT to directly compare seasonal root-zone soil water dynamics under managed plantation and native vegetation types (woodland and grassland) at the tree scale, in response to rainfall redistribution and root water uptake. Also, no studies have used surface ERT to estimate the deep drainage under these vegetation types to investigate the potential effect of plantation development on local groundwater resources.

Linking ERT resistivity data and soil water content requires the knowledge of petrophysical relationships. These empirical relationships are determined either from laboratory calibrations using field-collected soil samples (Brunet et al., 2010; Jayawickreme et al., 2010) or in-situ calibrations with point-scale TDR probes (Michot et al., 2003; Schwartz and Schreiber, 2009). Uncertainty is introduced due to the relatively small sample size and the altered conditions in soil structure and pore water salinity during laboratory experiments. Although field-calibrated relationships at the scale of ERT measurements are more reliable, only a few point measurements of water content from shallow soil depths are typically applied in relatively large model blocks to correlate electrical resistivity with water content (Michot et al., 2003; Schwartz and Schreiber, 2009). This may not be accurately representative of spatially averaged soil water in the model block. Spatial TDR is a novel method that can potentially provide the required soil water distribution with high spatial resolution. Spatial TDR determines continuous one-dimensional (1D) water content profiles along elongated sensors, based on the inversion of TDR measurements. Scheuermann et al. (2009) tested a spatial TDR system with 3-m-long flexible flat ribbon cables as sensors inside a full-scale dike model composed of uniform fine sands. They found that the spatial TDR was able to determine soil water distributions with a spatial resolution of about ±3 cm and an average absolute deviation of ±0.02 cm^3 cm^{-3}.

In subtropical coastal Australia, changes in vegetation cover, especially establishment of exotic pine plantations in areas of native banksia woodland and grassland, frequently occur with urban development and land use change. To understand the potential hydrological impacts of such changes, particularly those related to sustainable groundwater yields, we need to ascertain recharge for different vegetation covers and the spatial coverage with surface ERT can be useful for this purpose. In this paper, we quantified soil water dynamics in response to rainfall redistribution and water uptake by roots under three adjacent vegetation covers in a mixed sand dune forest by jointly using two different geophysical methods (surface ERT and spatial TDR). For our subtropical, sandy environment, the primary objectives are to: (1) evaluate the capability of spatial TDR and surface ERT to monitor 1D/2D water content distributions in sandy forest soils; (2) explore and compare seasonal dynamics of subsurface soil water under various vegetation types at the tree scale; (3) investigate how rainfall redistribution by canopy and root water uptake affect the spatial distribution of root-zone water content; and (4) estimate deep drainage under these vegetation types at this small spatial scale.

2. Materials and methods

2.1. Site description

Field observations were carried out in a sand dune area covered by open mixed forests mainly consisting of exotic slash pine (*Pinus elliottii* Engelm), native wallum Banksia (Banksia *aemula* R.Br.) and understory grass (*Lomandra elongata* Ewart) on North Stradbroke

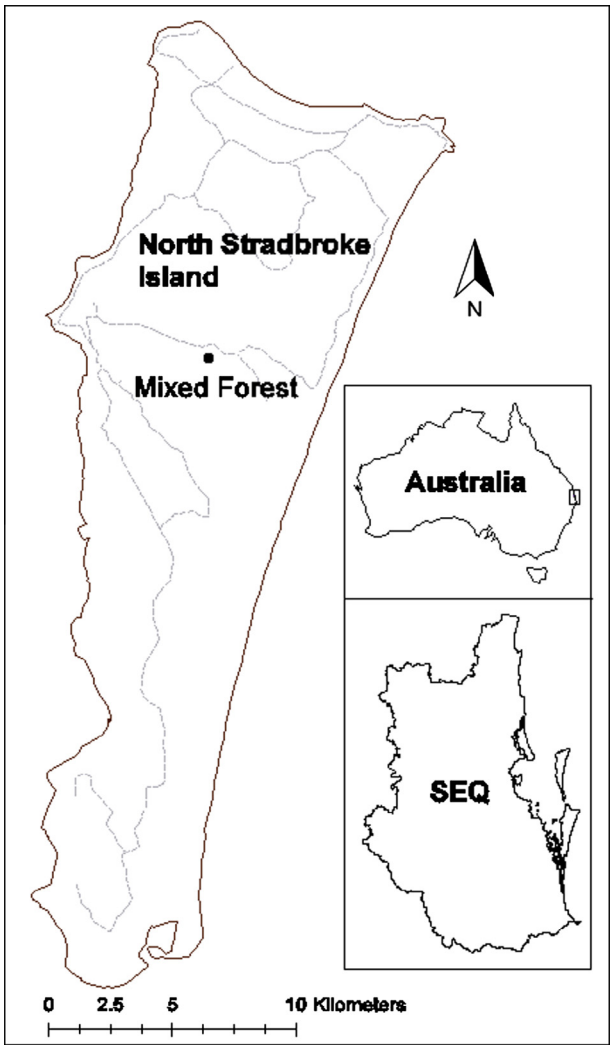

Fig. 1. Location map of the studied mixed forest in the sand dune on North Stradbroke Island, southeast Queensland (SEQ), Australia.

Island (27°30′40″S, 153°26′44″E), southeast Queensland, Australia (Fig. 1). North Stradbroke Island is the world's second largest sand island, with an area of ~280 km^2 and dune heights that ranged from 100 m to 150 m Australia Height Datum (Moss et al., 2013). The study site was a former pine plantation that was abandoned in year 2000. The pine trees reached an average height of 10.5 m and had an average stem diameter at breast height of 0.23 m. The banksia trees had a tree height of 5.3 m and a stem diameter of 0.20 m.

This area experiences a subtropical climate with a hot humid summer (December–February) and a mild dry winter (June–August). Over the one-year study period (November 2012–October 2013), the total annual rainfall amounted to 2200 mm (Fig. 2), which was higher than the long-term annual rainfall of 1600 mm (Australian Bureau of Meteorology). The average monthly air temperature ranged from 14 °C in July to 29 °C in January. The daily soil temperature measured at five depths with temperature sensors (type 107, Campbell Scientific, USA), varied from 12 °C to 29 °C at 10 cm depth and from 16 °C to 23 °C at 100 cm depth. At 400 cm depth, it remained ~19 °C throughout the year due to the damped response of deep soil temperature to surface air temperature. The depth to water table measured with a pressure transducer (Aqua Troll 200, In-Situ Inc., USA) varied between 8.42 m and 9.63 m during the study period (Fig. 2), with largest depth to water table occurring just before the onset of rainy period (end of January), and smallest depth to water table in mid-April. The sandy aquifer mainly consists of unconsolidated fine-grained sands based on soil-texture observations in three boreholes below the ERT transect after the geophysical surveys (Table 1). Soil water content logged with four probes (EC-5, Decagon Devices, USA) varied from 0.03 cm^3 cm^{-3} at 80 cm depth to 0.22 cm^3 cm^{-3} at 20 cm depth (Fig. 2).

2.2. Surface electrical resistivity tomography

2.2.1. Data acquisition

Between November 2012 and October 2013, 18 surface ERT surveys were conducted using a ten-channel SYSCAL Pro Switch resistivity meter (IRIS Instruments, France), of which 12 were presented here showing the seasonal soil water cycle. For electrical resistivity measurements, a total of 48 electrodes were permanently installed along a gentle slope (~12°) on the sand dune, regularly spaced at a horizontal interval of 0.5 m. The relative elevation of each electrode point was surveyed using a dumpy level and staff. The ERT

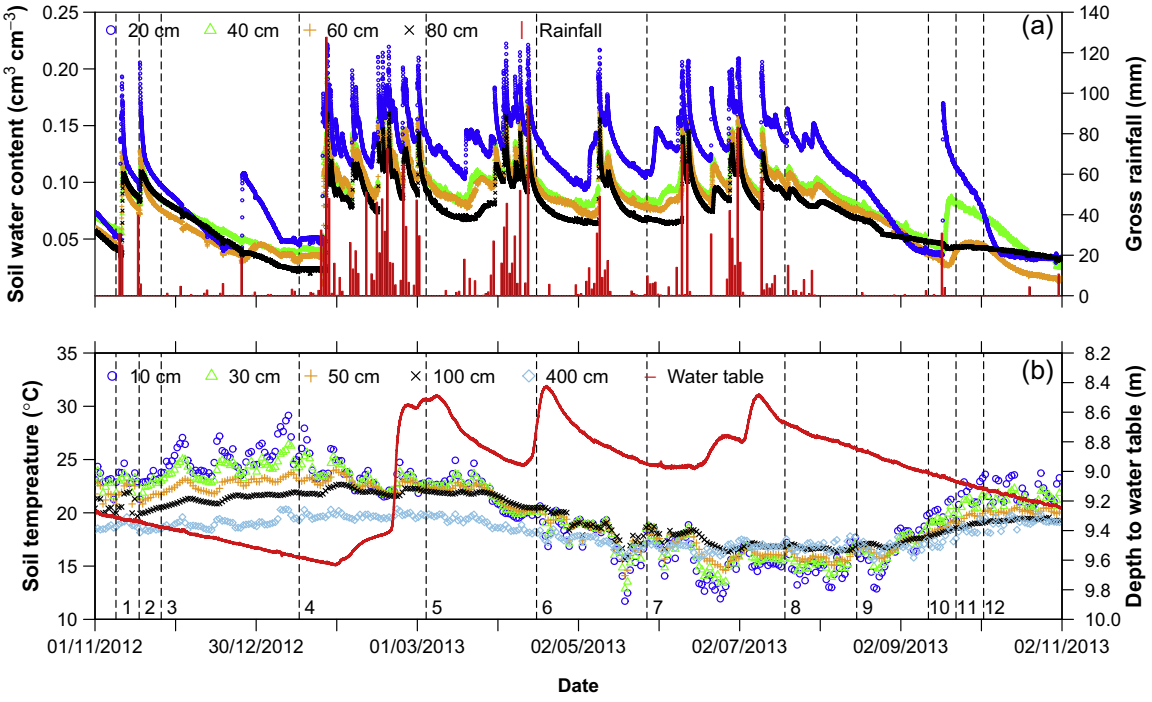

Fig. 2. (a) Time-series soil water content measured at four depths (20 cm, 40 cm, 60 cm and 80 cm) using point-scale soil water probes and daily gross rainfall; (b) soil temperature measured at five depths (10 cm, 30 cm, 50 cm, 100 cm and 400 cm) and water table fluctuation over the study period. Twelve dates for the surface ERT and spatial TDR surveys were indicated by the vertical dashed lines.

Table 1
Physical analyses of soil particle size distribution, bulk density (BD), saturated moisture content (θ_s) and saturated hydraulic conductivity (K_s) for soil samples from the field site. Soil properties were determined using intact samples from sand pits in upper 1.5 m of soil but using disturbed samples in lower 2.5 m of soil.

Depth (m)	Particle size distribution (%)			BD (g cm^{-3})	θ_s (cm^3 cm^{-3})	K_s (m d^{-1})
	50–100 μm	100–250 μm	250–500 μm			
0.2	29.0	60.5	10.5	1.42	0.33	2.54
0.5	34.1	57.5	8.4	1.45	0.31	1.68
1.0	17.2	68.4	14.4	1.51	0.29	1.10
1.5	31.6	59.8	8.6	1.52	0.28	1.57
2.0	43.9	44.9	11.2	1.55	0.31	2.06
3.0	18.8	65.3	15.9	1.50	0.28	2.34
4.0	24.7	64.6	10.7	1.56	0.30	1.33

transect along the downslope crossed a mixed pine–grass–banksia ecosystem (Fig. 3). Two-dimensional measurements of apparent soil resistivity were acquired with classic electrode configuration of Dipole-Dipole to take advantage of its highest spatial resolution and better depth coverage (Samouëlian et al., 2005). All ERT surveys were carried out in both normal and reciprocal modes to assess data quality (Koestel et al., 2008). To reduce contact resistance between the electrode and the soil under dry climatic conditions, the soils within a few centimeters around the electrodes were slightly wetted. Each measurement cycle contained 874 measurement points at 12 data levels with a maximum investigation depth of 4.0 m and took ~40 min to complete.

2.2.2. Data inversion

Prior to data inversion, the apparent resistivity data from the ERT measurements were filtered to remove noisy data. Data points with injected current less than 0.01 A or reciprocal errors larger than 5% were omitted from the inversion processes (Johnson et al., 2012; Wallin et al., 2013; Beff et al., 2013), which resulted in an elimination of 2% to 6% of measurement points collected from each dataset. To obtain the "true" subsurface resistivity distribution, we inverted the apparent resistivity data using the iterative tomographic inversion scheme of the RES2DINV software (Loke and Barker, 1995). To minimize artefacts produced by numerical inaccuracies from inverting each dataset separately, the time-lapse inversion method was applied which uses a common reference model to jointly invert datasets from different dates (Loke, 2013; Singha et al., 2014). We inverted the first dataset collected on 8 November 2012 to produce the starting and reference model for the subsequent time-lapse inversions, *i.e.* the same reference model was used for all the other datasets. A least-squares smoothness constraint was used to minimize the absolute changes in the model resistivity values between the initial model and the time-lapse model. Inversions of the datasets typically converged after 3–5 iterations, indicated by a change in root mean square error (RMSE) between consecutive iterations of less than 5%. Topographic corrections were also taken into account in the inversion processes. The topography data were incorporated into the modelling mesh and corrected using the distorted finite-element grid with the damped distortion method in the RES2DINV inversion software (Loke and Barker, 1995). We used a finite-difference mesh with a width of half the unit electrode spacing and a height of 25 cm at the surface, increasing by 6% for each deeper layer, which produced a total of 788 model blocks.

2.3. Spatial time domain reflectometry

To correlate soil electrical resistivity with soil water content, 1D soil water content distribution along flexible ribbon cables was monitored using spatial TDR (Scheuermann et al., 2009). The ribbon cables (6-cm-wide and 1-mm-thin) were made of three copper wires covered with polyethylene insulation. In June 2012, three such spatial TDR with 4-m-long ribbon cables were vertically installed in the soil along the ERT transect to ensure the comparability of surface ERT and spatial TDR (Fig. 3). To achieve this, boreholes (D = 12.5 cm) were drilled down to a depth of 4.0 m using a hand auger. The ribbon cables were manually pushed against one side of the augered boreholes. The coaxial cable, which was connected with the bottom end of the ribbon cable, was placed on the opposite side of the boreholes to avoid disturbance to the sensitive area of ribbon cables. To maintain original soil material and similar density for each soil layer, the boreholes were backfilled at 50 cm intervals with retrieved sands from corresponding layers. We started the spatial TDR measurements after a series of heavy rainfall events and a dry period in 2012, allowing the backfilled sands to consolidate naturally.

Spatial TDR measurements were performed from both ends of the ribbon cables to improve the spatial resolution. Through a multiplexer (SDMX50 Campbell Scientific), both ends of the ribbons were connected to a TDR device (Campbell Scientific TDR100) using a coaxial cable. Spatial TDR data were acquired immediately after each ERT survey. Spatially distributed capacitance (C) was firstly reconstructed with the measured TDR signals using the algorithm of Schlaeger (2005). Each reconstruction process took about three

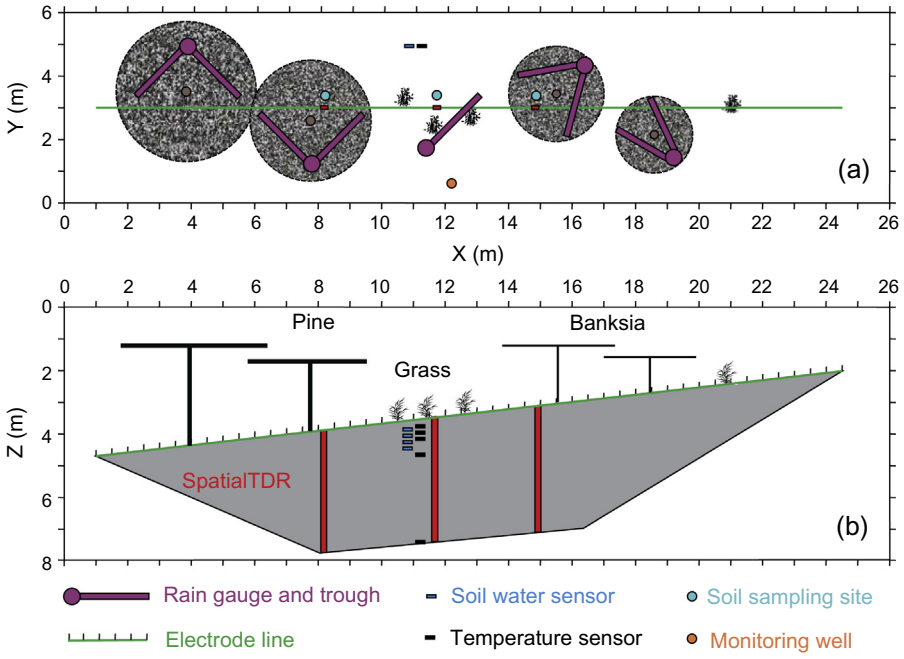

Fig. 3. Experimental field setup: (a) plan view and (b) elevation view, with positions of three contrasting vegetation types, ERT transect with 48 electrodes, three spatial TDR ribbons, five rain gauges and nine throughfall troughs, four soil water probes, five soil temperature sensors, three soil sampling sites and the monitoring well. The stippled circles represent the approximate tree canopy areas. Tree height was not scaled.

minutes to complete. Capacitance was then transformed to permittivity (ε_m) using the derived capacitance model (Scheuermann et al., 2009). Spatially distributed permittivity was finally converted into a volumetric water content (θ) profile along the insulated transmission line by a Topp-like equation (Topp et al., 1980) calibrated in the laboratory with field-collected soil samples ($\theta = -9.53 \times 10^{-2} + 4.11 \times 10^{-2}\,\varepsilon_m{}^{-1}.10 \times 10^{-3}\,\varepsilon_m{}^{2} + 5.51 \times 10^{-6}\,\varepsilon_m{}^{3}$, $R^2 = 0.9933$, $P < 0.01$, $n = 26$). The spatial TDR exhibited a spatial resolution of ±3 cm and a theoretical accuracy of ±0.02 $cm^3\ cm^{-3}$. Detailed information on the principle and inversion algorithm of the spatial TDR was previously presented by Scheuermann et al. (2009).

2.4. Petrophysical relationship between soil electrical resistivity and soil water content

Soil electrical resistivity depends on several soil properties, e.g., texture, porosity, pore water resistivity, soil water content, soil temperature and sometimes root biomass in vegetated soils (Samouëlian et al., 2005). During the study period, the measured electrical conductivities of rainwater and groundwater exhibited small variations (0.033 ± 0.007 S m^{-1} and 0.029 ± 0.005 S m^{-1}, respectively), indicating the electrical conductivity of pore water was relatively constant compared to the larger water content variations. Therefore, similar to other ERT studies (Michot et al., 2003; Brunet et al., 2010; Jayawickreme et al., 2010), we neglected the effect of pore water resistivity on soil electrical resistivity measurements.

Comparisons of electrical resistivity measurements require the expression of the electrical resistivity at a reference temperature, because temperature variations in the soil influence soil electrical resistivity. Seasonal soil temperature variations over depth were evident during the ERT surveys (Fig. 2), indicating that temperature correction was necessary. We assumed the temperature to be laterally uniform and temperature distribution was linearly interpolated over depth. To account for temperature effects, we corrected resistivity values after ERT data inversions with the equation by Keller and Frischknecht (1966) at a reference temperature of 25 °C:

$$\rho_{ref} = \rho_{soil}[1 + \alpha(T_{soil} - T_{ref})] \quad (1)$$

where ρ_{ref} (Ω m) is the corrected resistivity at a reference temperature T_{ref} (°C), usually 25 °C; ρ_{soil} (Ω m) is the inverted resistivity at soil temperature T_{soil} (°C) and α is the correction factor, equal to 0.025.

The petrophysical relationship linking soil electrical resistivity to water content was then applied to ρ_{ref} at 25 °C, using the simplified Archie's law (Yamakawa et al., 2012):

$$\rho_{ref} = A\theta^{-n} \quad (2)$$

where θ ($cm^3\ cm^{-3}$) is the soil water content, A is the empirical coefficient and n is the saturation exponent.

To estimate the fitting parameters, the temperature-corrected resistivities from ERT surveys were plotted against the water content values retrieved from spatial TDR during the first six surveys, while the spatial TDR measurements from the remaining surveys were used to validate the surface ERT-derived soil water content. For each measurement, the soil water content along spatial TDR cables were spatially averaged over each corresponding block depth of the inversion model to make the soil water content and electrical resistivity spatially comparable. Here, the vertical soil profile was divided into two layers: Top Layer (0–100 cm) and Bottom Layer (100–400 cm), considering that the majority (>90% of root biomass) of tree roots were found located in the upper 100 cm soil layer (Fan et al., 2015) and the soil properties (*e.g.* bulk density and porosity) were slightly different between the two soil layers (Table 1).

2.5. Additional measurements

The study site was equipped with a weather station located in a nearby clearing, which recorded gross rainfall, air temperature, relative humidity, solar radiation, wind direction and speed. To obtain net rainfall under tree canopies and in between trees, throughfall was collected using 9 U-shaped troughs connected to 5 HOBO RG3 tipping-bucket rain gauges (Onset Computer Corp., Bourne, USA). The troughs were made of split UPVC pipes, 2.5 m long by 0.1 m wide (Fig. 3). All the tipping-bucket rain gauges were calibrated to 0.2 mm per tip in the lab and recalibrated after deployments in the field (Llorens et al., 1997). Daily potential evapotranspiration (ET_p) was calculated following the Penman-Monteith method (Allen et al., 1998) using daily weather data. Transpiration of the pine and banksia trees was measured with the heat ratio method (HRM) sap flow sensors (ICT International Pty Ltd., Australia). Two HRM sensors (North and South cardinal direction) were installed at breast height (1.3 m above ground) on each tree. The individual tree sapwood area was derived from tree coring. Point measurements of sap flux density were scaled up to the tree scale by multiplying the local estimate of sap flux density by the sapwood area (Burgess et al., 2001). We assumed that the energy budget (solar radiation) under the trees was partitioned by the interception of tree canopy following Beer's law (Ritchie, 1972):

$$E = ET \cdot e^{-\beta \cdot LAI} \quad (3)$$

$$T = ET \cdot (1 - e^{-\beta \cdot LAI}) \quad (4)$$

where E (mm d^{-1}) is the soil evaporation, T (mm d^{-1}) is the tree transpiration, ET (mm d^{-1}) is the evapotranspiration, LAI ($m^2\ m^{-2}$) is the leaf area index, and β is the radiation extinction coefficient, equal to 0.4.

Based on Eqs. (3) and (4), the actual soil evaporation under trees was estimated using the sap flow-based transpiration and the measured leaf area index (LAI) under the pine (2.58 $m^2\ m^{-2}$) and banksia trees (2.34 $m^2\ m^{-2}$) with a LAI-2000 instrument (LI-COR Biosciences, Lincoln, NE). The actual ET for pine and banksia trees was then calculated as the sum of estimated soil evaporation and measured tree transpiration. The transpiration from the sparse grasses was considered to be minimal. Based on the estimated soil evaporation under the pine trees using the Beer's equation and the measured LAI under the pine trees and above the grasses (1.53 $m^2\ m^{-2}$), the actual soil evaporation under the grasses was estimated by assuming a simple inverse relation between E and LAI.

3. Results and discussion

3.1. Monitoring 1D vertical soil water content profile using spatial TDR

Fig. 4 presents several volumetric soil water content profiles along the three spatial TDR cables under the three vegetation covers. The continuous vertical distribution and seasonal evolution of soil water content were well captured by spatial TDR. The soil water content profiles measured using spatial TDR sensors under the pine, grass and banksia showed similar patterns but the magnitude varied as a function of depth and vegetation. Generally, higher soil water contents were observed under grasses than under pine and banksia trees, particularly in the upper 200 cm of soil.

At the beginning of the spatial TDR measurements (8 November 2012), all three monitored profiles exhibited a similar and

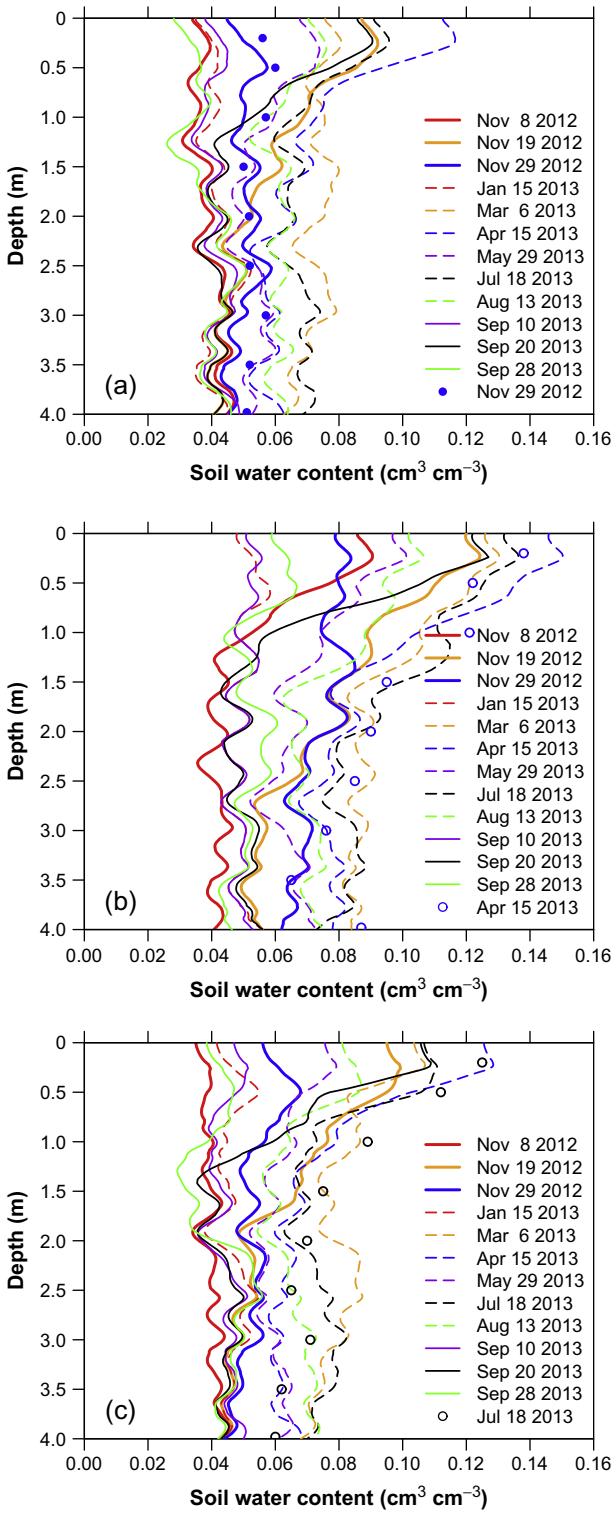

Fig. 4. One-dimensional soil water content profiles along three spatial TDR ribbons at different dates under three contrasting vegetation types: (a) pine, (b) grass and (c) banksia. Next to the spatial TDR data, point-scale soil water content values (solid circles) obtained from soil sampling at three different dates are shown.

relatively low soil water content (~0.04 cm^3 cm^{-3} averaged over 0–400 cm depth). For all vegetation types, an increase of the soil water content was observed on 19 November 2012 after three rainfall events, but the soil water content tended to decline to initial values following a dry period until 20 February 2013. The rates and amplitude of increase and decrease in soil water content varied depending on the vegetation type. During the wet season, the soil water was significantly replenished, ranging from 0.09 cm^3 cm^{-3} to 0.15 cm^3 cm^{-3} in the upper 100 cm soil and from 0.06 cm^3 cm^{-3} to 0.09 cm^3 cm^{-3} in the lower soil layers. However, the soil water was further depleted following the later dry period starting 10 September 2013. Between the first (8 November 2012) and the last (28 September 2013) spatial TDR surveys, soil water content in the whole soil profile was close to each other (Fig. 4).

To evaluate the performance of the spatial TDR measurements in the field, we compared continuous soil water content profiles measured by spatial TDR sensors with point-scale volumetric soil water content obtained by soil sampling at different depths (Fig. 5). Generally, the soil water content profile was well captured by the spatial TDR (Fig. 4). We obtained a good agreement between spatial TDR-derived and gravimetrically derived soil water content values (RMSE = 0.0112 cm^3 cm^{-3}, R^2 = 0.8577, n = 27), with deviations ranging from −0.0160 cm^3 cm^{-3} to 0.0158 cm^3 cm^{-3}. These differences were expected since the soil sampling sites were 0.3 m from the locations of spatial TDR ribbons. The maximum absolute deviation was less than 0.02 cm^3 cm^{-3}, which was comparable with the accuracy of other available TDR and capacitance sensors, e.g., TDR 100 (~2%, Campbell Scientific, USA) and EC-5 (2–3%, Decagon Devices, USA). However, the evolution of soil water content over certain observation periods varied around 2%, especially in the bottom soil layers, which was close to the accuracy of the spatial TDR. In order to lower the errors of soil water content estimates in this environment, it would be useful to integrate the spatial soil water content profile over certain depths (*e.g.* 10 cm) to obtain the area-average soil water content. The undulations in the measured soil water content profiles are most likely caused by the differences in the density of different backfilled soil layers since the spikes corresponded to the interfaces of the backfilled soil layers. No obvious undulations were identified by Scheuermann et al. (2009) in their homogeneously constructed dike model probably because the spatial TDR sensors were installed in the uniform sands compared to our natural sands in that specific sand dune environment.

Installation of soil water sensors in vertical boreholes is likely to change the soil structure and properties, which may produce preferential flow and not be representative of natural soil water content measurements (Dahan et al., 2007). For unconsolidated fine sands in this study, although slight changes in soil density is

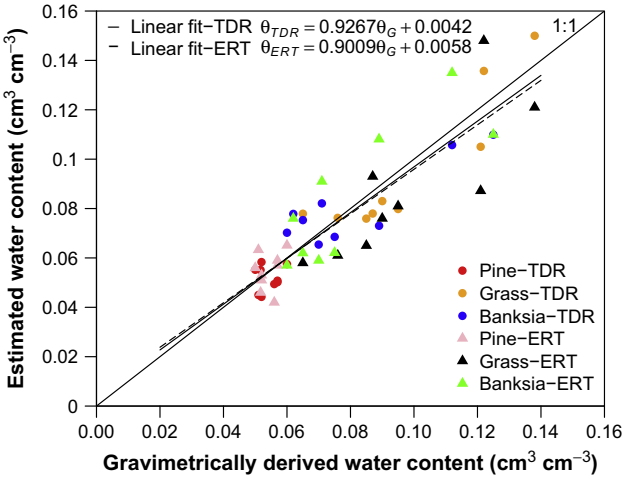

Fig. 5. Comparisons between gravimetrically derived soil water content (θ_G) and those derived by spatial TDR (θ_{TDR}) and surface ERT (θ_{ERT}) under different vegetation types.

expected, it is possible to allow soils being measured in a minimally disturbed condition after natural soil reorganization. However, a proper installation method is required for other heavy-textured materials to permit soil to be measured with minimum disturbance (Scheuermann et al., 2009). Dahan et al. (2007) developed a technique for the attachment of capacitance probes on flexible sleeves, which was inserted into angled boreholes and filled with liquid resin to press the sensors against the borehole walls. This method could be applicable for installation of our ribbon cables in the slanted boreholes.

3.2. Mapping spatial variation of soil electrical resistivity using surface ERT

The subsurface sensitivity of 2D ERT inversion model produced by the RES2DINV software (Loke and Barker, 1995) is given in Fig. 6. The sensitivity variations across the ERT image were obvious. The sensitivity of the ERT measurement decreased as the depth of investigation increased, indicating loss of resolution at the bottom of the ERT image. The sensitivity was relatively high in the top 1.5 m layers, where most of the important hydrological processes occurred. The image resolution in the bottom layers was not as high as that in the surface layers, but the reliability of the resistivity measurements was still good given a higher data point coverage in these layers. Although the sensitivity of ERT measurements to local soil electrical resistivity changes was lower at the bottom of the soil layers, spatial TDR measurements showed that the soil water variations were also smaller at these depths (Fig. 4). The lower resolution in the bottom layers was thus considered to be less important in this study.

Fig. 7 presents the spatial variations of the temperature-corrected soil electrical resistivity monitored during various ERT surveys. The data inversion models produced generally lower error statistics (RMSE <2%) during the wet season than those during the dry season (RMSE = 2–4%) most likely due to the improved current movement by a better soil electrical conductivity. Very high electrical resistivity was observed at the beginning of the ERT surveys, ranging between 5000 Ω m and 9000 Ω m. Specifically, the higher resistivities extended deeper (~2.5 m) under the pine trees than under the other two vegetation types. A similar pattern was observed for banksia but restricted to the top 1.5 m. On 19 November 2012, regions with resistivity <4000 Ω m were observed in the upper soils and resistivity in other areas of the soil fell inside the range of approximately 4000 to 5000 Ω m. On 29 November 2012, regions with resistivity <3700 Ω m were observed under the grasses in the middle part of the soil profile. On 15 January, resistivity values in most of the soil profile region were between 5500 Ω m and 6500 Ω m, although patchy anomalies with higher resistivity (>7500 Ω m) were still observed under the pine tree. During the rainy season, much lower soil electrical resistivity was observed, particularly in the upper 1 m soil layer (<2500 Ω m), indicating the effect of rainfall on soil resistivity. Contrarily to the top layer, the electrical resistivity was slightly higher at greater depth (2500–4000 Ω m). On 29 May and 13 August 2013, the resistivity profiles were almost the same with lower resistivity near the surface. On 10 September 2013, similar resistivity distribution was observed as that at the beginning of the measurements. During the last two ERT measurements, relative uniform resistivities (4500–5500 Ω m) were observed within the whole soil profile, except for the lower resistivity near the surface and patches of extreme resistivity zones (~10,000 Ω m) observed under pine trees.

Generally, soil resistivities taken under the pine trees were greater than those under the banksia trees, followed by those under the grassland. These differences were particularly obvious during dry periods. Higher values of soil resistivity under the pine and banksia trees can be related to lower soil water content levels resulting from higher soil water depletion by deep-rooted woody vegetation (Jayawickreme et al., 2008; Garré et al., 2012). Jayawickreme et al. (2008) found that higher evapotranspiration caused a high increase in root-zone soil resistivity below the mature Maple forest compared to the grassland. The obvious resistivity differences in the top soil layers under different vegetation covers are also likely due to the higher woody root biomass under the trees which can significantly affect the soil resistivity (Amato et al., 2008; Rossi et al., 2011). Rossi et al. (2011) observed large resistivity values close to tree trunks in an orchard and the variability in resistivity was positively related to the belowground biomass density of coarse roots (>2 mm diameter).

3.3. Conversion of soil electrical resistivity into soil water content

We used the temperature-corrected soil electrical resistivity data and soil water content from spatial TDR to establish the site-specific relationships between the two variables for the two soil layers (Fig. 8). For Top Layer (0–100 cm) and Bottom Layer (100–400 cm), we obtained two significantly different petrophysical relationships with the parameters of the simplified Archie's model ($P < 0.05$). The optimized parameters were $A = 218.9$, $n = 1.068$ for Top Layer and $A = 172.4$, $n = 1.175$ for Bottom Layer. The determined parameter n was within the low range of typical values (1.0–2.7) for unconsolidated sands (Ulrich and Slater, 2004). The fit for Archie's law in the first layer ($R^2 = 0.921$, RMSE = 0.013, $n = 54$) is slightly better than the second layer ($R^2 = 0.851$, RMSE = 0.019, $n = 162$). These correlations suggest that surface ERT can be used to quantitatively evaluate temporal

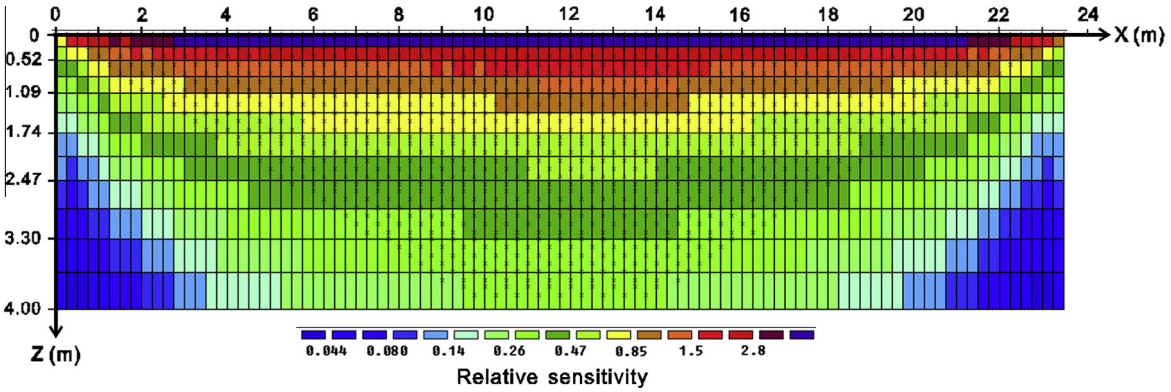

Fig. 6. Sensitivity map of ERT for each model block generated from the imported geometry of the electrodes and inversion parameters used in this study.

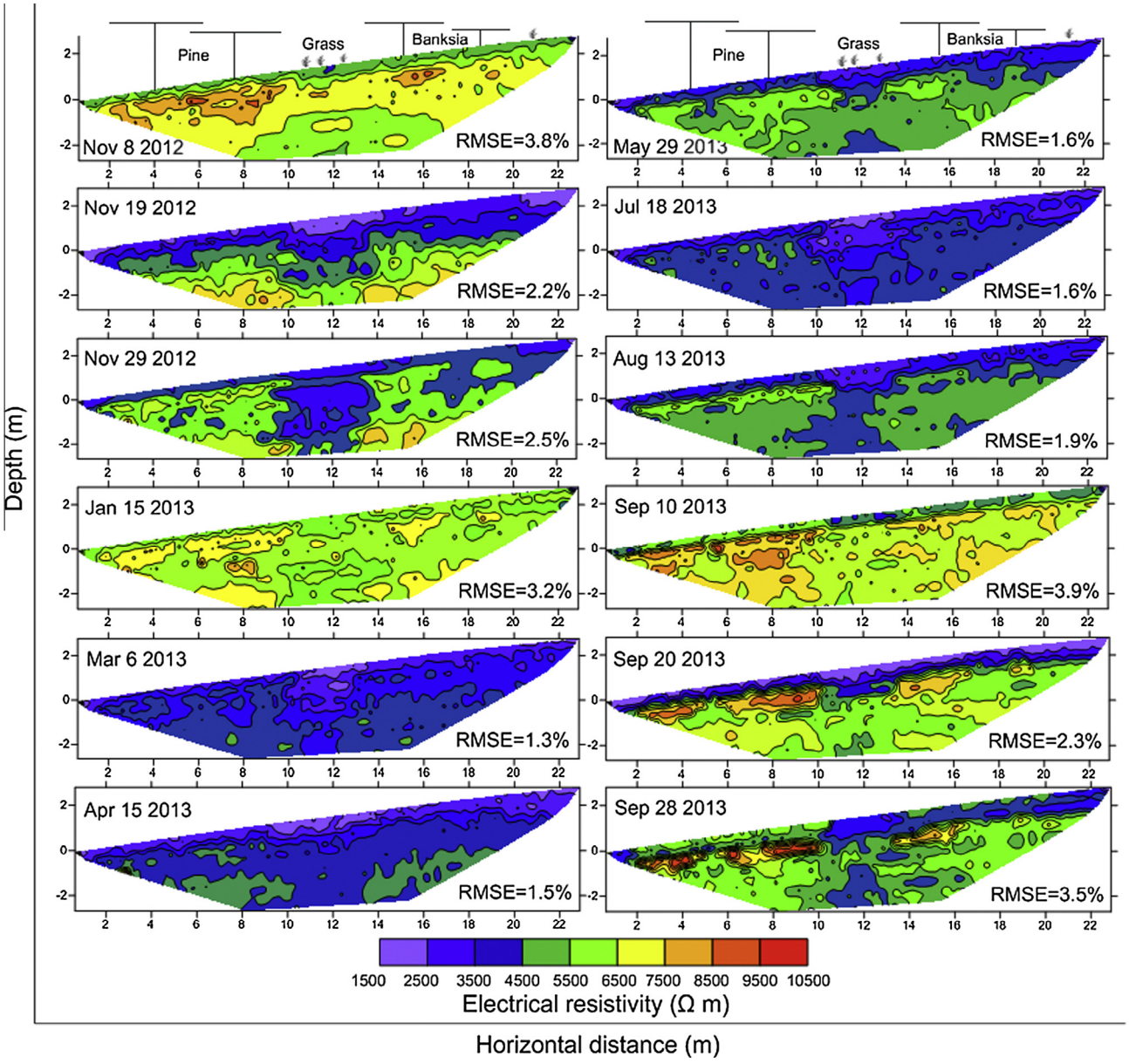

Fig. 7. Two-dimensional spatial variations of the temperature-corrected soil electrical resistivity monitored during 12 various ERT surveys.

variations in soil water content using the field-calibrated relationships between the spatial TDR-derived soil water content and the surface ERT-derived soil electrical resistivity.

As expected, soil electrical resistivity decreases as soil water content increases. As seen from the fitted curve, for soil water contents <0.10 $cm^3\ cm^{-3}$, the electrical resistivity rapidly decreases with increasing soil water content. However, at high soil water contents (>0.15 $cm^3\ cm^{-3}$) only very little change in resistivity is observed when the soil water content increases or decreases, which indicates an accurate estimation of higher soil water content can be difficult using the petrophysical functions. As found by other laboratory and field studies (Fukue et al., 1999; Michot et al., 2003; Samouëlian et al., 2005), the soil water content threshold between low and high electrical resistivity variation was around 0.15–0.20 $cm^3\ cm^{-3}$. However, the natural soil water content in the sand dunes during our ERT surveys generally changes at small and medium soil water contents (0.03–0.15 $cm^3\ cm^{-3}$) compared with saturated soil water content of ~0.30 $cm^3\ cm^{-3}$. Soil water content measurements at shallow soil depths confirmed that the soil water content seldom exceeded 0.20 $cm^3\ cm^{-3}$ due to a low water holding capacity and a fast percolation (Fig. 2).

The first soil layer exhibited larger variations of soil water content than the second soil layer. The measured resistivity at the same soil water content for the first layer was smaller than that for the second layer, particularly in the high resistivity range. This can be due to the differences in root biomass and soil properties between the two soil layers. Werban et al. (2008) observed two distinct petrophysical relationships in presence or absence of fine roots of lupine. In contrast, Beff et al. (2013) found no obvious improvement on calibration of petrophysical functions when splitting the data into that with and without the presence of roots. The root surface area, especially for mature tree roots, was considered relatively non-conductive due to the presence of highly insulating materials such as cell-wall components and voids (Rossi et al.,

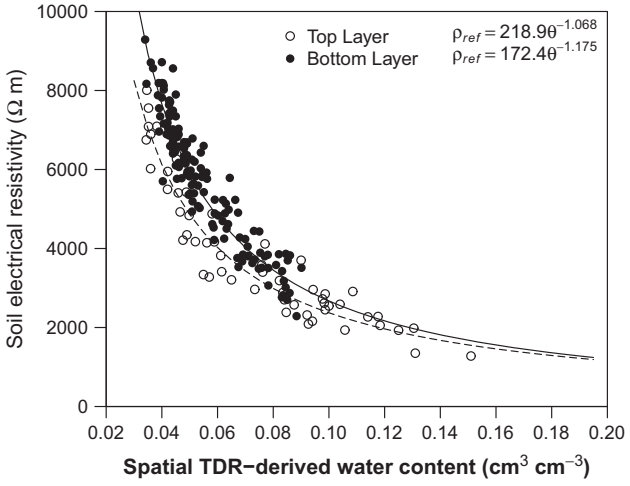

Fig. 8. Relationship between soil electrical resistivity (ρ_{ref}) and spatially averaged water content (θ) obtained from spatial TDR for Top Layer and Bottom Layer.

2011; Furman et al., 2013). However, tree roots can potentially affect the soil resistivity measurements due to the high water content and solute concentrations in the root xylem (Amato et al., 2008; Nadler and Tyree, 2008).The root biomass was expected to exert more effect at high resistivity, and at lower values the response of resistivity to roots was too weak to be discriminated from the effect of variations of other soil properties (Amato et al., 2008). Besides, this difference can be caused by the higher soil porosity (Fig. 2) and potentially higher organic matter in the top soil layers, which tended to retain more soil water and thus lower the electrical resistivity. This difference can also result from differences in the salt concentration between two soil layers. The surface soils are expected to contain higher salts due to the soil evaporation processes and are thus more conductive than the bottom soils.

3.4. Comparison between soil water content obtained by surface ERT and spatial TDR

To verify the quality of the surface ERT measurements for the two soil layers, we compared the soil water content measured by the surface ERT and the spatial TDR during the last six surveys whose data were not used for establishing the site-specific relationships (Fig. 9). We obtain a reasonably good agreement between ERT-derived and TDR-derived soil water content values (Top Layer: RMSE = 0.0154 cm^3 cm^{-3}, R^2 = 0.88, n = 54; Bottom Layer: RMSE = 0.0182 cm^3 cm^{-3}, R^2 = 0.73, n = 162). This difference is similar to the error associated with the calibrated petrophysical relationships. The estimate precision quantified by RMSE indicates that the surface ERT-derived soil water content for the second layer is worse than that for the first layer, with a maximum absolute deviation of 0.028 cm^3 cm^{-3} for the bottom 100 cm soil layer. The mean error (ME) values of −0.0075 cm^3 cm^{-3} (Top Layer) and 0.0043 cm^3 cm^{-3} (Bottom Layer) indicated that surface ERT generally underestimated soil water content in the upper 100 cm of soil but slightly overestimated soil water content in the deeper layer.

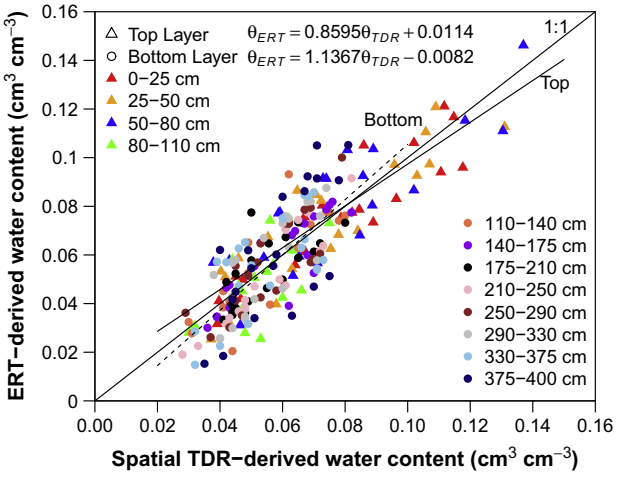

Fig. 9. Comparison of soil water content derived by surface ERT (θ_{ERT}) and average soil water content measured by spatial TDR (θ_{TDR}) for Top Layer and Bottom Layer during the last six ERT surveys. The dashed and solid lines represent the linear regressions.

We also obtained a reasonable agreement between ERT-derived and gravimetrically derived water content values (RMSE = 0.0173 cm^3 cm^{-3}, R^2 = 0.7892, n = 27, Fig. 5), with deviations ranging from −0.0338 cm^3 cm^{-3} to 0.0260 cm^3 cm^{-3} and an average absolute deviation of 0.0119 cm^3 cm^{-3}. The slightly higher deviations for the surface ERT than for the spatial TDR measurements can be largely explained by the decrease in resolution with depth of ERT signal and associated smoothing artifacts from inversion (LaBrecque et al., 1996; Marescot et al., 2003). However, these introduced errors appeared lower than generally reported values in other surface ERT-based water content studies. For example, Brunet et al. (2010) compared the soil water content obtained from ERT with local measurements made with TDR at ten different times and found absolute deviations up to 0.05 cm^3 cm^{-3}. Michot et al. (2003) reported a high RMSE of 0.036 cm^3 cm^{-3} and a ME of 0.0145 cm^3 cm^{-3} for their ERT-based estimates of water content. In the above studies, the soil type, electrode array and spacing, calibration method of petrophysical relationship were different from this study. Calibration of the petrophysical relationship using spatial TDR with more calibration points, especially covering all depths of the soil profile could improve the quality of this relationship and hence produced smaller errors. However, the lower errors of measured water content may be ascribed to our relatively uniform fine sands in the sand dune environment compared to the more heterogeneous clayey and loamy soils in other studies.

3.5. Quantifying 2D distribution and seasonal evolution of soil water content

Two-dimensional soil water content distributions over time were determined using the temperature-corrected ERT sections and the petrophysical relationships for the two soil layers. Differences in spatial soil water content distribution under various vegetation types and seasonal root-zone water content were obvious during the study period (Fig. 10). The root-zone soil was very dry during the two dry periods (November 2012 to January 2013, August to October 2013) but replenished by rainfall events during the wet season (February to July 2013), with an average wet-season soil water content of ~0.09 cm^3 cm^{-3} for the entire vertical soil profile. Two-dimensional soil water content distributions showed distinct variations in the soil water content between the three vegetation covers, with relatively lower soil water content under pine trees than those under grasses and banksia trees.

At the beginning of the ERT campaign (8 November 2012), following a dry period from August to October in 2012, the estimated soil water content across the site was quite low and relatively uniform, averaged at ~0.04 cm^3 cm^{-3}. On 19 November 2012, after three rainfall events (total rainfall 100 mm), the water content was partly replenished, mainly in the upper 1.5 m of soil. The water content then gradually declined until the end of this dry period, prior to the beginning of the wet season. A series of high

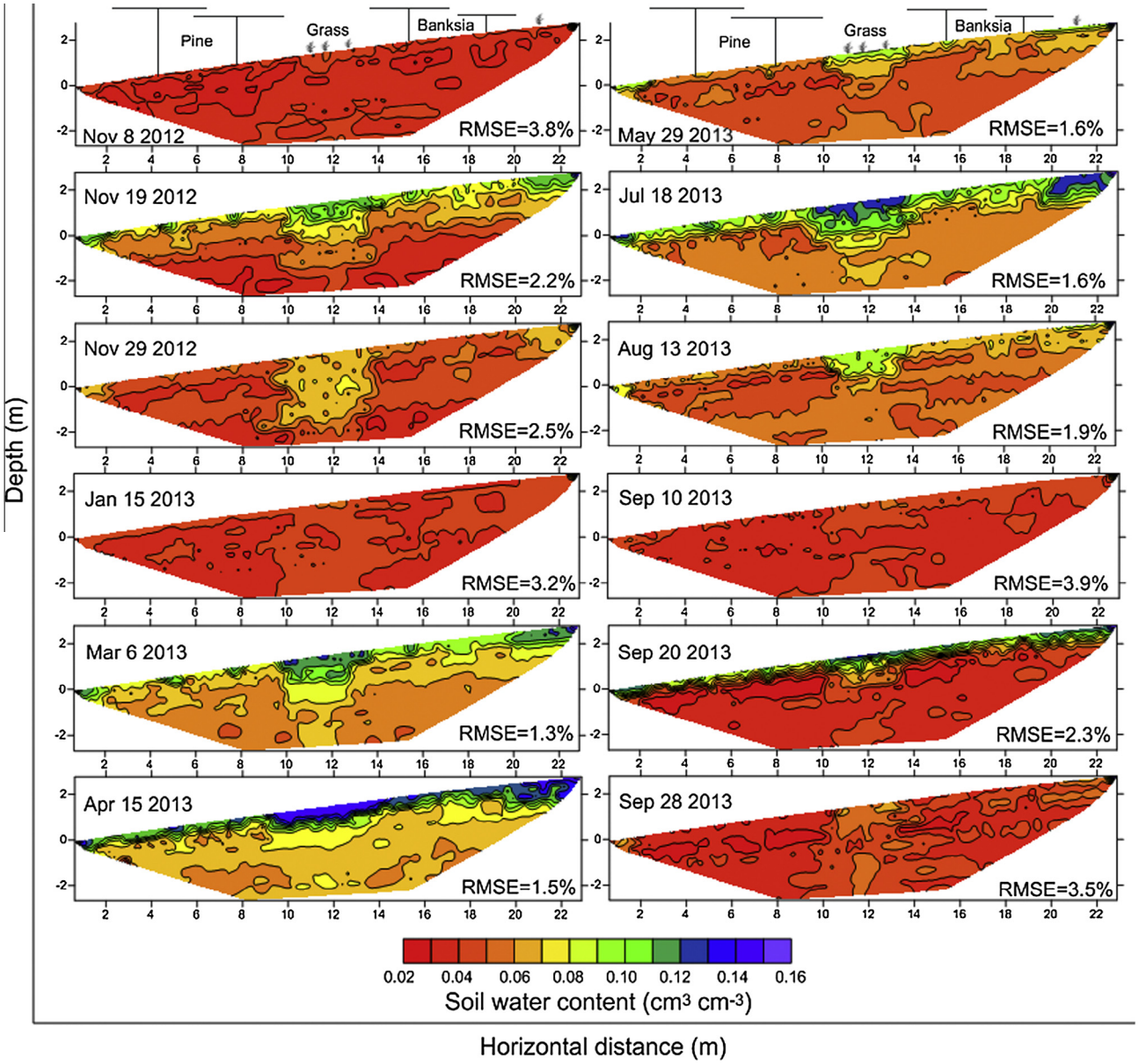

Fig. 10. Two-dimensional spatial variations of the soil water content monitored during 12 various ERT surveys.

intensity rainfall events over the next month (total rainfall 300 mm) significantly replenished the soil, ranging from 0.08 cm^3 - cm^{-3} at a depth of 4.0 m to 0.15 cm^3 cm^{-3} at soil surface. During March–April 2012, a large portion of rainfall percolated through the vadose zone, reached the water table and recharged the groundwater (Fig. 2). The soil water content stayed high over the subsequent four months due to replenishment by periodic rainfall events, with the highest soil water content in mid-April 2013. Following a further dry period from May to June 2013, the soil water content significantly decreased, particularly at the top layers (1 m). At the end of the ERT measurements, the water content over the soil profile declined toward its initial level, except for the slightly higher surface water content which was due to a recent rainfall event in September 2013.

These results revealed obvious variations of soil water content along the ERT transect, so a better observation strategy was needed to obtain the area-average water content when using the soil water balance method to investigate hydrological processes in forested ecosystems. To achieve this, we calculated 2D area-average soil water storage from surface ERT and 1D soil water storage from spatial TDR under different vegetation types for the 12 ERT survey dates (Table 2). The soil water storage was obtained by integrating surface ERT-derived water content and spatial TDR-derived water content from 0 to 400 cm depth, respectively. The corresponding surface transects for the pine, grass and banksia segments were 2–10 m, 10–14 m and 14–20 m, respectively. Absolute and relative differences between the 2D and 1D water storage values were also determined. The calculated differences in soil water storage were large and ranged between −44 mm (−15.6%) under the pine trees and 46 mm (15.5%) under the banksia trees. The soil water storage difference was relatively smaller under the grassland, with a maximum deviation of 19 mm (6.1%). Larger deviations of soil water content under the trees likely resulted from the higher spatial variability of soil water caused by canopy rainfall redistribution and root water uptake.

These differences indicated that estimating the area-average soil water content at the tree scale with one soil water content monitoring profile, especially with several point-scale probes,

Table 2
Difference (ΔS, mm) between 1D soil water storage estimated by spatial TDR (S_{TDR}, mm) and 2D area-average soil water storage estimated by surface ERT (S_{ERT}, mm) on different survey dates. The values in the parenthesis represent the relative difference (%) as a ratio between the soil water storage difference and surface ERT-derived soil water storage.

Date	Pine			Grass			Banksia		
	S_{ERT}	S_{TDR}	ΔS	S_{ERT}	S_{TDR}	ΔS	S_{ERT}	S_{TDR}	ΔS
D1	183	162	−21 (−11.4)	218	216	−2 (−0.9)	179	189	10 (5.7)
D2	250	220	−30 (−11.9)	310	301	−9 (−2.9)	252	288	36 (14.4)
D3	203	186	−17 (−8.3)	297	288	−9 (−3.0)	217	237	20 (9.3)
D4	168	161	−7 (−3.9)	200	212	12 (6.0)	187	193	6 (3.3)
D5	294	267	−27 (−9.1)	388	403	15 (4.0)	330	357	27 (8.3)
D6	279	235	−44 (−15.6)	378	386	8 (2.2)	298	344	46 (15.5)
D7	226	203	−23 (−10.3)	287	275	−12 (−4.0)	250	287	37 (14.8)
D8	284	243	−41 (−14.4)	392	389	−3 (−0.7)	316	319	3 (0.9)
D9	253	228	−25 (−9.7)	315	334	19 (6.1)	275	289	14 (5.2)
D10	160	148	−12 (−7.6)	195	187	−8 (−4.1)	168	187	19 (11.5)
D11	170	164	−6 (−3.6)	219	210	−9 (−4.1)	187	225	38 (20.5)
D12	156	142	−14 (−9.1)	214	212	−2 (−0.9)	174	197	23 (13.4)
Total	2625	2359	−266 (−10.1)	3411	3413	2 (0.1)	2831	3112	281 (9.9)

was not straightforward. The results supported the use of surface ERT to quantify the spatial variability of soil water content and to guide the installation locations of soil water sensors to obtain more accurate estimates of area-average soil water content in the forest. Both spatial TDR and surface ERT enabled the measurements of soil water content of sandy forest soils down to a depth of 4 m, which is the maximum rooting depth for the majority of vegetation types (Canadell et al., 1996). This capability makes them very useful for the detection of root zone processes and predicting the deep drainage with the soil water balance method by combining the rainfall and ET measurements in forested ecosystems. With spatial TDR measurements, the dynamics of continuous soil water distribution can be successfully monitored with high spatial resolution and accuracy, but the distribution is limited to one dimension. It is therefore advantageous to combine spatial TDR with surface ERT measurements to quantify the spatial distribution of soil water (both laterally and in depth) since they can complement each other with spatial resolution and coverage, respectively.

3.6. Comparison of deep drainage under different vegetation types

Fig. 11 shows the evolution of the calculated potential *ET*, the sap flow-based actual *ET* for pine and banksia trees, and the proportionally estimated actual *ET* for grasses at the study plot. During the experimental period, the daily potential *ET* generally decreased from summer (December–February) to winter (June–August) as the atmospheric evaporative demand was lower in the winter (Fig. 2). The potential *ET* first gradually decreased from ~6 mm d^{-1} in November 2012 to ~2 mm d^{-1} in June 2013, and then increased to a value of ~7 mm d^{-1} in November 2013. The estimated actual *ET* rates for pine trees were generally larger than the corresponding values of the banksia trees, followed by the grassland. During the rainy period (February–August 2013), the estimated actual *ET* rates for all vegetation types were closer to the corresponding potential *ET* values. However, the estimated actual *ET* rates during the dry periods (December 2012–January 2013 and September–November 2013) were approximately one-third of the corresponding potential *ET* values, indicating the significant limiting effect of soil water content on actual *ET* (Fig. 2).

The water balance components under different vegetation types for 11 periods between our 12 surface ERT surveys are presented in Table 3. Runoff was considered to be minimal given the lower rainfall intensity compared to hydraulic conductivity of surface soil and the fast percolation of near-surface soil water into lower soil layers. Total annual deep drainage under the grasses accumulated to 1502 mm over the one-year study period (Table 3), representing 69% of the annual gross rainfall. Based on the water table fluctuation method (Scanlon et al., 2002), gross recharge estimated under the grassland over the year was estimated as 950 mm using a readily available specific yield of 0.30 (Loheide et al., 2005), representing 45% of gross rainfall. The difference between surface ERT-derived deep drainage and the water table fluctuation-derived gross recharge was largely due to the uncertainties obtained from other water balance terms, especially the *ET* estimate for the small scale of the grassland. The estimated deep drainage under the pine trees was only half of that under the grass, and also lower than that of the banksia trees due to its high rainfall interception and root water uptake, indicating the negative effect of pine planation establishment on groundwater recharge in these areas. However, the water table fluctuations indicate that a large portion of rainfall

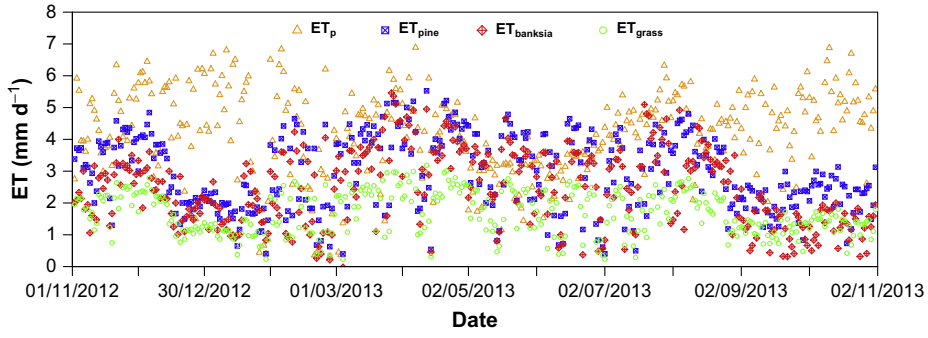

Fig. 11. Evolution of the calculated potential evapotranspiration (ET_p), the sap flow-based actual evapotranspiration for pine (ET_{pine}) and banksia ($ET_{banksia}$) trees, and the proportionally estimated actual evapotranspiration for grasses (ET_{grass}) over the study period.

Table 3
Water balance components estimated under different vegetation types (pine, grass and banksia) at the studied small spatial scale for 11 periods between the 12 surface ERT survey dates.

Period	Pine				Grass				Banksia			
	ΔS	ET_a	P_n	DD	ΔS	ET_a	P_n	DD	ΔS	ET_a	P_n	DD
Nov 8–Nov 19 2012	67	34	78	−23	92	19	96	−15	73	26	84	−15
Nov 19–Nov 29 2012	−47	40	0	7	−13	16	0	−3	−35	31	0	4
Nov 29 2012–Jan 15 2013	−35	118	33	−49	−97	68	42	71	−30	91	36	−25
Jan 15–Mar 6 2013	126	131	666	409	188	76	819	556	143	110	717	465
Mar 6–Apr 15 2013	−15	140	303	178	−10	81	370	300	−32	134	327	225
Apr 15–May 29 2013	−52	158	139	33	−91	91	174	174	−48	142	149	55
May 29–Jul 18 2013	58	137	374	179	105	79	461	278	66	126	402	210
Jul 18–Aug 13 2013	−31	95	36	−28	−77	55	41	63	−41	89	39	−8
Aug 13–Sep 10 2013	−86	72	4	19	−116	41	5	83	−95	67	4	32
Sep 10–Sep 20 2013	14	19	27	−2	24	11	34	−1	19	13	29	−3
Sep 20–Sep 28 2013	−10	15	0	−5	−5	9	0	−4	−13	12	0	1
Total	−11	959	1660	718	0	546	2042	1502	7	841	1787	941

ΔS: difference in soil water storage; ET_a: actual evapotranspiration; P_n: net rainfall (gross rainfall minus interception loss); DD: deep drainage.

still percolated beyond the root zone following a series of heavy summer storms and reached groundwater table (Fig. 2) due to the high saturated hydraulic conductivity (~180 cm d^{-1}) of our unconsolidated dune sands compared to heavy-textured soils.

3.7. Effect of rainfall redistribution and root water uptake on soil water content heterogeneity

To obtain a better understanding of the effects of rainfall redistribution by canopy and water uptake by roots on soil water variability and the potential of this monitoring approach, we quantified the differences in 2D soil water content during two short-term (~10 d) wetting and drying cycles (Fig. 12), i.e., W1 (8–19 November 2012, rainfall = 100 mm), D1 (19–29 November 2012), W2 (10–20 September 2013, rainfall = 30 mm) and D2 (20–28 September 2013).

After a cumulative rainfall of 100 mm during W1 and 30 mm during W2, an increase of soil water content in the soil profile was observed with surface ERT for both periods (Fig. 12). The increase was mainly located under grasses, followed by the banksia and pine trees. Specifically, the differences in soil water storage over the whole soil profile during W1 were 67 mm, 92 mm and 73 mm under pine, grassland and banksia trees, respectively. The corresponding values during W2 were 14 mm, 24 mm and 19 mm, respectively. As we can see from Table 3, these differences were mainly due to the combined effect of the higher surface water input and smaller soil water loss via *ET* under the grass zone. Similar to our earlier finding (Fan et al., 2014), we found that the pine trees intercepted more rainfall (24.3% of gross rainfall) than the banksia trees (18.5% of gross rainfall), while the rainfall interception by the sparse grasses was smaller (5.4% of gross rainfall). The reduced amount of infiltrating rainwater under the trees was ascribed to their higher interception losses. However, a locally higher increase in soil water content was identified around all tree trunks except for one banksia tree, reaching similar levels of soil water content to that under the grasses. This was similar to findings by Michot et al. (2003) who identified preferential infiltration of rainwater under corn plants caused by stemflow, which tended to homogenize the soil water content under the corn row and under the inter-row when a significant rainfall occurred. During the field trips, we have also observed stemflow running down along the tree barks and concentrated around the bases of pine and banksia trees. We considered that the stemflow of pine and banksia trees in this study were similar to our previous findings

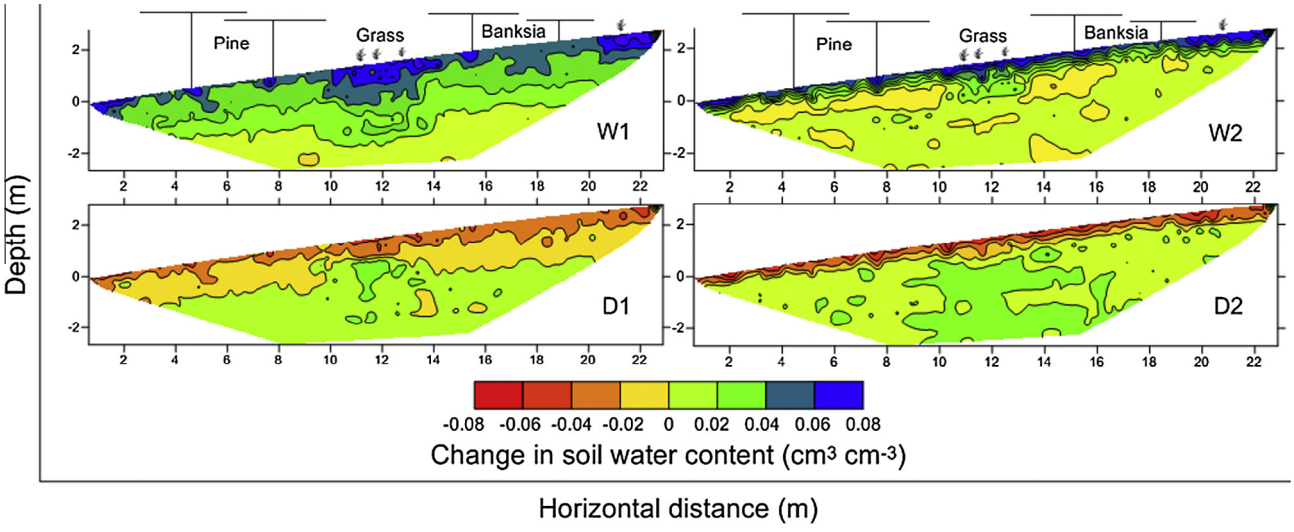

Fig. 12. Two-dimensional soil water evolutions during wetting and drying cycles: W1 (8–19 November 2012), D1 (19–29 November 2012), W2 (10–20 September 2013), and D2 (20–28 September 2013). Zero means no changes in the soil water content during the comparison periods. Values above or below zero indicate an increase or a decrease in soil water content during each comparison period, respectively.

on the same tree species (Fan et al., 2014), with higher stemflow under the pine trees (1.0% of gross rainfall) than that under the banksia trees (0.4% of gross rainfall). No localized increase was found around the grasses due to its negligible stemflow. No increase in soil water content was identified around the base of one banksia tree most likely due to its relatively smaller portion of stemflow water and the ERT transect being located 0.8 m from its trunk. The stemflow has been generally found to concentrate within a radius of less than 0.5 m from the tree trunk (Cattan et al., 2009; Nikodem et al., 2010).

During the drying periods D1 and D2, ET caused a decrease of water content in the soil profile. The differences in water storage throughout the soil profile during D1 were −47 mm, −13 mm and −35 mm under pine, grassland and banksia trees, respectively. The corresponding values during D2 were −10 mm, −5 mm and −13 mm, respectively. Since deep drainage at the bottom boundary was limited during these periods (Table 3) due to the small water pressure gradient at the bottom of the soil, these differences were ascribed to the *ET* processes. In the upper 1 m soil of the tree area, higher water depletion was observed around the tree trunks relative to the intercanopy area. This is similar to Michot et al. (2003) who also observed a higher decrease of water content under the corn rows due to root water uptake. However, Srayeddin and Doussan (2009) found the soil water decreased mainly under the inter-rows in the upper 1 m of soil, because the water content at the surface and under the corn rows was relatively low and water depletion occurred in the deeper zones and in the inter-row area. These results indicated that both spatial rainfall distribution (*e.g.* throughfall and stemflow) and root water uptake were influencing the patterns of soil water content and its variation over time as well as the infiltrating water under different vegetation types at our study site.

4. Conclusions

Geophysical instruments are becoming increasingly attractive for high-resolution investigation of subsurface flow processes with minimized disturbance to soils. In this study, we used 2D surface ERT, supplemented by 1D spatial TDR, to monitor root-zone water dynamics of sand dune soils in a subtropical coastal environment. Spatial variation was primarily due to rainfall partitioning by vegetation and root uptake under three vegetation types at the site. The resulting 2D ERT images exhibited clear horizontal and vertical variations of soil electrical resistivity, which were quantitatively related to soil water content changes with in-situ calibrated petrophysical relationships using spatial TDR data. Soil water content evolutions throughout the year were successfully identified by soil electrical resistivity changes. Soil temperature and topographic variations were also accounted for during the ERT data interpretation.

Analysis of field resistivity and soil water content between November 2012 and October 2013 confirmed the potential of surface ERT and spatial TDR for use in monitoring spatial and temporal water dynamics of sand dune soils. Relative to traditional point-scale TDR probes, spatial TDR can provide continuous 1D water content measurements with high spatial resolution and accuracy (absolute deviation <0.02 $cm^3\ cm^{-3}$). With a series of continuous soil water content profiles, percolation of wetting front through the root zone can be well traced. In comparison with spatial TDR, surface ERT gives 2D information integrated over a greater volume of soil. In our case, the measurements have reasonable accuracy (RMSE <0.02 $cm^3\ cm^{-3}$) compared with soil sampling methods. However, a slightly higher error in soil water measurements was introduced in the bottom soil layers probably due to the lower sensitivity of ERT measurements to local soil electrical resistivity changes at these depths. Combination of surface ERT and spatial TDR methods can improve the overall accuracy of soil water monitoring with a better spatial resolution than obtained separately or by point methods. Better positioning of point-scale soil water sensors can be guided by surface ERT for area-average soil water content estimates in heterogeneous forests.

The rainwater infiltration after canopy redistribution, the drying out of the soil by root water uptake, the preferential flow by stemflow and the surface drainage of the soil water could be identified by joint use of surface ERT and spatial TDR methods. The rainfall interception by the canopy played a major role in redistribution of water at the soil surface before it infiltrated into the soil since it reduced the net rainfall input on the floor under different vegetation types (75.7%, 81.7% and 94.6% of gross rainfall for pine, banksia and grass, respectively). During the heavy rainfall events in the wet season, the effect of the root water uptake on deep drainage appeared to be limited at this highly conductive sand dune site as a result of the fast percolation of rainwater beyond the root zone. The estimated annual deep drainage under the pine trees (718 mm) was only half of that under the grass (1502 mm), and also lower than that under the banksia trees (941 mm) due to its high rainfall interception and root water uptake, indicating the negative effect of pine plantation establishment on local groundwater recharge in these areas. Vegetation cover changes from native ecosystems (banksia and grasses) to exotic pine plantation in these sand dune areas are likely to reduce the soil water content and the subsequent recharge in the underlying aquifer.

Acknowledgments

This study was financially sponsored by the National Centre for Groundwater Research and Training (NCGRT), co-funded by the Australian Research Council and the National Water Commission. The project was also supported by a Queensland Science Fellowship awarded to A. Scheuermann. We acknowledge the insightful suggestions from the associate editor and four anonymous reviewers. Special thanks are given to Jeremy Canard for his assistance in the field installation and observations.

References

Amato, M., Basso, B., Celano, G., Bitella, G., Morelli, G., Rossi, R., 2008. In situ detection of tree root distribution and biomass by multi-electrode resistivity imaging. Tree Physiol. 28, 1441–1448.

Allen, R.G., Pereira, L.S., Raes, D., Smith, M., 1998. Crop Evapotranspiration-Guidelines for Computing Crop Water Requirements-FAO Irrigation and Drainage Paper 56. FAO, Rome, 300, 6541.

Beff, L., Günther, T., Vandoorne, B., Couvreur, V., Javaux, M., 2013. Three-dimensional monitoring of soil water content in a maize field using Electrical Resistivity Tomography. Hydrol. Earth Syst. Sci. 17, 595–609.

Bosch, J.M., Hewlett, J.D., 1982. A review of catchment experiments to determine the effect of vegetation changes on water yield and evapotranspiration. J. Hydrol. 55, 3–23.

Brillante, L., Bois, B., Mathieu, O., Bichet, V., Michot, D., Lévêque, J., 2014. Monitoring soil volume wetness in heterogeneous soils by electrical resistivity. A field-based pedotransfer function. J. Hydrol. 516, 56–66.

Brunet, P., Clément, R., Bouvier, C., 2010. Monitoring soil water content and deficit using Electrical Resistivity Tomography (ERT) – a case study in the Cevennes area, France. J. Hydrol. 380, 146–153.

Burgess, S.S., Adams, M.A., Turner, N.C., Beverly, C.R., Ong, C.K., Khan, A.A., Bleby, T.M., 2001. An improved heat pulse method to measure low and reverse rates of sap flow in woody plants. Tree Physiol. 21 (9), 589–598.

Calamita, G., Brocca, L., Perrone, A., Piscitelli, S., Lapenna, V., Melone, F., Moramarco, T., 2012. Electrical resistivity and TDR methods for soil moisture estimation in central Italy test-sites. J. Hydrol. 454, 101–112.

Canadell, J., Jackson, R.B., Ehleringer, J.B., Mooney, H.A., Sala, O.E., Schulze, E.-D., 1996. Maximum rooting depth of vegetation types at the global scale. Oecologia 108, 583–595.

Cattan, P., Ruy, S.M., Cabidoche, Y.-M., Findeling, A., Desbois, P., Charlier, J.B., 2009. Effect on runoff of rainfall redistribution by the impluvium-shaped canopy of banana cultivated on an Andosol with a high infiltration rate. J. Hydrol. 368, 251–261.

Dahan, O., Shani, Y., Enzel, Y., Yechieli, Y., Yakirevich, A., 2007. Direct measurements of floodwater infiltration into shallow alluvial aquifers. J. Hydrol. 344, 157–170.

Fan, J., Guyot, A., Oestergaarda, K., Lockington, D., 2014. Measuring and modeling rainfall interception losses by a native Banksia woodland and an exotic pine plantation in subtropical coastal Australia. J. Hydrol. 515, 156–165.

Fan, J., Baumgartl, T., Scheuermann, A., Lockington, D., 2015. Modelling effects of canopy and roots on soil moisture and deep drainage. Vadose Zone J. http://dx.doi.org/10.2136/vzj2014.09.0131.

Ferré, P.A., Knight, J.H., Rudolph, D.L., Kachanoski, R.G., 1998. The sample areas of conventional and alternative time domain reflectometry probes. Water Resour. Res. 34 (11), 2971–2979.

Ford, C.R., Hubbard, R.M., Vose, J.M., 2011. Quantifying structural and physiological controls on variation in canopy transpiration among planted pine and hardwood species in the southern Appalachians. Ecohydrology 4, 183–195.

French, H., Binley, A., 2004. Snowmelt infiltration: monitoring temporal and spatial variability using time-lapse electrical resistivity. J. Hydrol. 297, 174–186.

Fukue, M., Minato, T., Horibe, H., Taya, N., 1999. The micro-structures of clay given by resistivity measurements. Eng. Geol. 54, 43–53.

Furman, A., Arnon-Zur, A., Assouline, S., 2013. Electrical resistivity tomography of the root zone. Soil Water Root Proc. Adv. Tomogr. Imaging, 223–245.

Garré, S., Günther, T., Diels, J., Vanderborght, J., 2012. Evaluating experimental design of ERT for soil moisture monitoring in contour hedgerow intercropping systems. Vadose Zone J. 11 (4).

Huisman, J.A., Hubbard, S.S., Redman, J.D., Annan, A.P., 2003. Measuring soil water content with ground penetrating radar. Vadose Zone J. 2, 476–491.

Jayawickreme, D.H., Van Dam, R.L., Hyndman, D.W., 2008. Subsurface imaging of vegetation, climate, and root-zone moisture interactions. Geophys. Res. Lett. 35, L18404.

Jayawickreme, D.H., Van Dam, R.L., Hyndman, D.W., 2010. Hydrological consequences of land-cover change: quantifying the influence of plants on soil moisture with time-lapse electrical resistivity. Geophysics 75, WA43–WA50.

Johnson, T.C., Slater, L.D., Ntarlagiannis, D., Day-Lewis, F.D., Elwaseif, M., 2012. Monitoring groundwater-surface water interaction using time-series and time-frequency analysis of transient three-dimensional electrical resistivity changes. Water Resour. Res. 48, W07506.

Keller, G.V., Frischknecht, F.C., 1966. Electrical Methods in Geophysical Prospecting.

Koestel, J., Kemna, A., Javaux, M., Binley, A., Vereecken, H., 2008. Quantitative imaging of solute transport in an unsaturated and undisturbed soil monolith with 3-D ERT and TDR. Water Resour. Res. 44, W12411.

LaBrecque, D.J., Ramirez, A.L., Daily, W.D., Binley, A.M., Schima, S.A., 1996. ERT monitoring of environmental remediation processes. Meas. Sci. Technol. 7 (3), 375.

Lehmann, P., Gambazzi, F., Suski, B., Baron, L., Askarinejad, A., Springman, S.M., Holliger, K., Or, D., 2013. Evolution of soil wetting patterns preceding a hydrologically induced landslide inferred from electrical resistivity survey and point measurements of volumetric water content and pore water pressure. Water Resour. Res. 49, 7992–8004.

Llorens, P., Poch, R., Latron, J., Gallart, F., 1997. Rainfall interception by a *Pinus sylvestris* forest patch overgrown in a Mediterranean mountainous abandoned area I. Monitoring design and results down to the event scale. J. Hydrol. 199, 331–345.

Loheide, S.P., Butler, J.J., Gorelick, S.M., 2005. Estimation of groundwater consumption by phreatophytes using diurnal water table fluctuations: a saturated-unsaturated flow assessment. Water Resour. Res. 41, W07030.

Loke, M.H., 2013. Rapid 2-D resistivity & IP inversion using the least-squares method. Man. Res2dinv, Version 3, p. 71.

Loke, M.H., Barker, R.D., 1995. Least-squares deconvolution of apparent resistivity pseudosections. Geophysics 60, 1682–1690.

Marescot, L., Loke, M.H., Chapellier, D., Delaloye, R., Lambiel, C., Reynard, E., 2003. Assessing reliability of 2D resistivity imaging in mountain permafrost studies using the depth of investigation index method. Near Surf. Geophys. 1, 57–67.

Michot, D., Benderitter, Y., Dorigny, A., Nicoullaud, B., King, D., Tabbagh, A., 2003. Spatial and temporal monitoring of soil water content with an irrigated corn crop cover using surface electrical resistivity tomography. Water Resour. Res., 39

Moss, P.T., Tibby, J., Petherick, L., McGowan, H., Barr, C., 2013. Late quaternary vegetation history of north Stradbroke Island, Queensland, eastern Australia. Quat. Sci. Rev. 74, 257–272.

Nadler, A., Tyree, M.T., 2008. Substituting stem's water content by electrical conductivity for monitoring water status changes. Soil Sci. Soc. Am. J. 72, 1006–1013.

Nikodem, A., Kodešová, R., Drábek, O., Bubeníčková, L., Boruvka, L., Pavlu, L., Tejnecky, V., 2010. A numerical study of the impact of precipitation redistribution in a beech forest canopy on water and aluminum transport in a Podzol. Vadose Zone J. 9, 238–251.

Ritchie, J.T., 1972. Model for predicting evaporation from a row crop with incomplete cover. Water Resour. Res. 8 (5), 1204–1213.

Robinson, D.A., Abdu, H., Lebron, I., Jones, S.B., 2012. Imaging of hill-slope soil moisture wetting patterns in a semi-arid oak savanna catchment using time-lapse electromagnetic induction. J. Hydrol. 416–417, 39–49.

Robinson, D.A., Campbell, C.S., Hopmans, J.W., Hornbuckle, B.K., Jones, S.B., Knight, R., Wendroth, O., 2008. Soil moisture measurement for ecological and hydrological watershed-scale observatories: a review. Vadose Zone J. 7 (1), 358–389.

Rossi, R., Amato, M., Bitella, G., Bochicchio, R., Ferreira Gomes, J.J., Lovelli, S., Martorella, E., Favale, P., 2011. Electrical resistivity tomography as a non-destructive method for mapping root biomass in an orchard. Eur. J. Soil Sci. 62 (2), 206–215.

Samouëlian, A., Cousin, I., Tabbagh, A., Bruand, A., Richard, G., 2005. Electrical resistivity survey in soil science: a review. Soil Tillage Res. 83, 173–193.

Scanlon, B.R., Healy, R.W., Cook, P.G., 2002. Choosing appropriate techniques for quantifying groundwater recharge. J. Hydrol. 10 (1), 18–39.

Scheuermann, A., Huebner, C., Schlaeger, S., Wagner, N., Becker, R., Bieberstein, A., 2009. Spatial time domain reflectometry and its application for the measurement of water content distributions along flat ribbon cables in a full-scale levee model. Water Resour. Res., 45

Schlaeger, S., 2005. A fast TDR-inversion technique for the reconstruction of spatial soil moisture content. Hydrol. Earth Syst. Sci. Discuss. Discuss. 2, 971–1009.

Schwartz, B.F., Schreiber, M.E., 2009. Quantifying potential recharge in mantled sinkholes using ERT. Ground Water 47, 370–381.

Schwartz, B.F., Schreiber, M.E., Yan, T., 2008. Quantifying field-scale soil moisture using electrical resistivity imaging. J. Hydrol. 362, 234–246.

Singha, K., Day-Lewis, F.D., Johnson, T., Slater, L.D., 2014. Advances in interpretation of subsurface processes with time-lapse electrical imaging. Hydrol. Process.

Srayeddin, I., Doussan, C., 2009. Estimation of the spatial variability of root water uptake of maize and sorghum at the field scale by electrical resistivity tomography. Plant Soil 319, 185–207.

Steelman, C.M., Endres, A.L., Jones, J.P., 2012. High-resolution ground-penetrating radar monitoring of soil moisture dynamics: field results, interpretation, and comparison with unsaturated flow model. Water Resour. Res. 48, W09538.

Topp, G.C., Davis, J.L., Annan, A.P., 1980. Electromagnetic determination of soil water content: measurements in coaxial transmission lines. Water Resour. Res. 16, 574–582.

Ulrich, C., Slater, L., 2004. Induced polarization measurements on unsaturated, unconsolidated sands. Geophysics 69, 762–771.

Vereecken, H., Huisman, J.A., Bogena, H., Vanderborght, J., Vrugt, J.A., Hopmans, J.W., 2008. On the value of soil moisture measurements in vadose zone hydrology: a review. Water Resour. Res., 44

Vereecken, H., Huisman, J.A., Pachepsky, Y., Montzka, C., van der Kruk, J., Bogena, H., Weihermüller, L., Herbst, M., Martinez, G., Vanderborght, J., 2013. On the spatio-temporal dynamics of soil moisture at the field scale. J. Hydrol. 516, 76–96.

Wallin, E.L., Johnson, T.C., Greenwood, W.J., Zachara, J.M., 2013. Imaging high stage river-water intrusion into a contaminated aquifer along a major river corridor using 2-D time-lapse surface electrical resistivity tomography. Water Resour. Res. 49, 1693–1708.

Werban, U., Attia al Hagrey, S., Rabbel, W., 2008. Monitoring of root-zone water content in the laboratory by 2D geoelectrical tomography. J. Plant Nutr. Soil Sci. 171, 927–935.

Western, A.W., Grayson, R.B., Blöschl, G., Wilson, D.J., 2003. Spatial variability of soil moisture and its implications for scaling. In: Pachepsky, Y., Radcliffe, D.E., Magdi Selim, H. (Eds.), Scaling Methods Soil Phys. CRC Press.

Yamakawa, Y., Kosugi, K., Katsura, S., Masaoka, N., Mizuyama, T., 2012. Spatial and temporal monitoring of water content in weathered granitic bedrock using electrical resistivity imaging. Vadose Zone J. 11.

Zhang, L., Dawes, W.R., Walker, G.R., 2001. Response of mean annual evapotranspiration to vegetation changes at catchment scale. Water Resour. Res. 37, 701–708.

Zhou, Q.Y., Shimada, J., Sato, A., 2001. Three-dimensional spatial and temporal monitoring of soil water content using electrical resistivity tomography. Water Resour. Res. 37, 273–285.